Hindawi Publishing Corporation
Journal of Applied Mathematics
Volume 2013, Article ID 856171, 8 pages
http://dx.doi.org/10.1155/2013/856171

Research Article

Simulation of Stress Distribution near Weld Line in the Viscoelastic Melt Mold Filling Process

Binxin Yang,[1] Jie Ouyang,[2] and Fang Wang[1]

[1] *School of Applied Sciences, Taiyuan University of Science and Technology, Taiyuan, Shanxi 030024, China*
[2] *School of Science, Northwestern Polytechnical University, Xi'an, Shaanxi 710072, China*

Correspondence should be addressed to Jie Ouyang; jieouyang@nwpu.edu.cn

Received 20 April 2013; Revised 31 May 2013; Accepted 18 June 2013

Academic Editor: Bo Yu

Simulations of interface evolution and stress distribution near weld line in the viscoelastic melt mold filling process are achieved according to the viscoelastic-Newtonian two-phase model. The finite volume methods on nonstaggered grids are used to solve the model. The level set method is used to capture the melt interface. The interface evolution of the viscoelastic melt in the mold filling process with an insert in is captured accurately and compared with the result obtained in the experiment. Numerical results show that the stress distribution is anisotropic near the weld line district and the stress distribution varies greatly at different positions of the weld line district due to the complicated flow behavior after the two streams of melt meet. The stress increases quickly near the weld line district and then decreases gradually until reaching the tail of the mold cavity. The maximum value of the stress appears at some point after the insert.

1. Introduction

The plastic mold filling process produces large numbers of parts of high quality. Plastic material in the form of granules is melted until it is soft enough to be injected under pressure to fill a mold. Early simulations of mold filling process mostly used the Hele-Shaw model coupled with the finite element method, which is based on the creeping flow lubrication model [1–4]. With the development of computer hardware, 3D simulations of mold filling process have been realized by using Navier-Stokes equations and different numerical methods [5–10]. The papers mentioned above studied the mold filling process without the consideration of the interface motion. The development of the interface capturing or tracking techniques, such as volume of fluid method (VOF) and the level set method has propelled greatly the development of mold filling simulation techniques. Many papers studying mold filling process coupled with interface tracking techniques can be found [11–20]. In these papers, the viscoelastic properties of materials were ignored. However, the melt for mold filling process is often viscoelastic materials. Some papers made a study on mold filling problems with viscoelastic free surfaces [21, 22]. However, these papers studied the problem with only viscoelastic fluid phase considered and the gas phase in the cavity ignored, in which case complex boundary conditions must be properly dealt with. Yang et al. [23] proposed a model for mold filling process in which the governing equations for the viscoelastic fluid (melt phase) and the Newtonian fluid (gas phase) are successfully united into a system of generalized Navier-Stokes equations, avoiding dealing with complex boundary conditions.

The viscoelastic behaviour in mold filling process has been tested in [23], in which the die swelling phenomenon and the influences of elasticity and viscosity on velocity, stresses, pressure, stretch, and the first normal-stress difference have been discussed in detail. However, it is well known that weld line is unavoidable in most products of even moderate complexity by mold filling process and influences weightily the quality of the products and the stress distribution near the weld line influences the mechanical property of the products greatly. This paper uses the viscoelastic-Newtonian two-phase flow model established in [23] and finite volume method on nonstaggered grids to study the mold filling process with an insert in the cavity and analyze the stress distribution near the weld line. The comparison

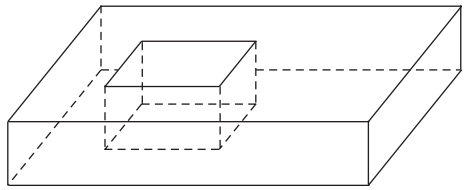

Figure 1: Sketch map of the mold with an insert in.

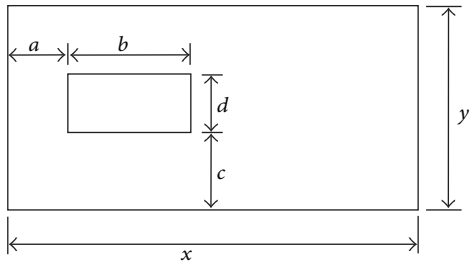

Figure 2: Computational domain of the mold.

between the numerical results and those obtained from experiments shows the correctness of the model and the numerical methods.

2. Mathematical Model (see [23])

2.1. Interface Capturing Equations. We use the corrected level set method proposed by Sussman et al. [27] to capture the interface. The level set and its reinitialization equations are described as follows:

$$\frac{\partial \varphi}{\partial t} + \mathbf{u} \cdot \nabla \varphi = 0 \tag{1}$$

$$\begin{aligned} &\frac{\partial \varphi}{\partial t_r} + \operatorname{sign}(\varphi_0)\left(\left|\nabla \varphi\right| - 1\right) = \omega \delta_\varepsilon(\varphi)\left|\nabla \varphi\right|, \\ &\varphi(x, y, 0) = \varphi_0(x, y), \end{aligned} \tag{2}$$

where φ is the interface, $\mathbf{u} = (u, v)$ is the velocity vector of the melt, t is the time, ω is the weight coefficient, t_r is a pseudo time, and $\operatorname{sign}(\varphi_0)$ is the sign function of φ which is defined as

$$\operatorname{sign}(\varphi_0) = \frac{\varphi_0}{\sqrt{\varphi_0^2 + \left[\min(\Delta x, \Delta y)\right]^2}}. \tag{3}$$

Here, Δx and Δy are the grid widths along x and y direction, respectively, and $[\min(\Delta x, \Delta y)]^2$ is used to avoid denominator's dividing by zero. $\delta_\varepsilon(\varphi)$ is the Dirac function defined as

$$\delta_\varepsilon(\varphi) = \begin{cases} \dfrac{1}{2\varepsilon}\left(1 + \cos\left(\dfrac{\pi \varphi}{\varepsilon}\right)\right) & |\varphi| < \varepsilon, \\ 0 & \text{otherwise.} \end{cases} \tag{4}$$

Here, ε is a small positive number about a grid width. See Sussman et al. [27] for more details.

2.2. Governing Equations for Flow Field. The governing equations for the flow field with the consideration of fibers are given as follows.

Continuity

$$\frac{\partial \rho}{\partial t} + \frac{\partial u}{\partial x} + \frac{\partial v}{\partial y} = 0, \tag{5}$$

u-momentum

$$\begin{aligned} &\frac{\partial(\rho u)}{\partial t} + \frac{\partial(\rho u u)}{\partial x} + \frac{\partial(\rho v u)}{\partial y} - \frac{1}{\mathrm{Re}}\left(\frac{\partial^2(\mu u)}{\partial x^2} + \frac{\partial^2(\mu u)}{\partial y^2}\right) \\ &\quad = -\frac{\partial p}{\partial x} H_\varepsilon(\varphi) + \frac{(\beta - 1)}{\mathrm{Re}}\left(\frac{\partial^2(\mu u)}{\partial x^2} + \frac{\partial^2(\mu u)}{\partial y^2}\right) H_\varepsilon(\varphi) \\ &\qquad + \frac{1}{\mathrm{Re}}\frac{\partial \tau_{xx}}{\partial x} H_\varepsilon(\varphi) + \frac{1}{\mathrm{Re}}\frac{\partial \tau_{xy}}{\partial y} H_\varepsilon(\varphi), \end{aligned} \tag{6}$$

v-momentum

$$\begin{aligned} &\frac{\partial(\rho v)}{\partial t} + \frac{\partial(\rho u v)}{\partial x} + \frac{\partial(\rho v v)}{\partial y} - \frac{1}{\mathrm{Re}}\left(\frac{\partial^2(\mu v)}{\partial x^2} + \frac{\partial^2(\mu v)}{\partial y^2}\right) \\ &\quad = -\frac{\partial p}{\partial y} H_\varepsilon(\varphi) + \frac{(\beta - 1)}{\mathrm{Re}}\left(\frac{\partial^2(\mu v)}{\partial x^2} + \frac{\partial^2(\mu v)}{\partial y^2}\right) H_\varepsilon(\varphi) \\ &\qquad + \frac{1}{\mathrm{Re}}\frac{\partial \tau_{yx}}{\partial x} H_\varepsilon(\varphi) + \frac{1}{\mathrm{Re}}\frac{\partial \tau_{yy}}{\partial y} H_\varepsilon(\varphi), \end{aligned} \tag{7}$$

where the Reynolds number $\mathrm{Re} = \rho_l L U / \mu_l$, $\rho(\varphi) = \xi + (1 - \xi) H_\varepsilon(\varphi)$, $\mu(\varphi) = \eta + (1 - \eta) H_\varepsilon(\varphi)$, $\xi = \rho_g / \rho_l$, $\eta = \mu_g / \mu_l$, β is the ratio of the Newtonian viscosity and the total viscosity. Since isothermal mold filling process is considered here, β is a constant. The subscripts l and g denote the liquid phase and the gas phase, respectively, and L and U are parameters for nondimensionalization.

Constitutive

$$\omega \frac{\partial \psi}{\partial t} + \nabla \cdot (\omega \mathbf{u} \psi) - \nabla \cdot (\Lambda \nabla \psi) = S_\psi. \tag{8}$$

Here, the extended Pom-Pom (XPP) constitutive equation developed by Verbeeten et al. [28] is used as the constitutive relationship. The constants and functions in (8) are defined in Table 1 [24, 25], where $f(\lambda, \boldsymbol{\tau}) = 2\lambda_{0b}/\lambda_{0s} e^{\nu(\lambda - 1)}(1 - 1/\lambda) + 1/\lambda^2[1 - \alpha \mathbf{I}_{\tau \cdot \tau}/3G_0^2]$, $\lambda = \sqrt{1 + |\mathbf{I}_\tau|/3G_0}$, $\nu = 2/q$, and the Weissenberg number is defined as $\mathrm{We} = \lambda_{0b} U / L$. Here λ is the backbone stretch used to represent the stretched degree of the polymer molecule, λ_{0b} and λ_{0s} denote the orientation and backbone stretch relaxation time scales of the polymer chains, respectively, G_0 is the linear relaxation modulus, α is an adjustable parameter, which controls the anisotropic drag, $\mathbf{I}$ is the identity tensor, q is the number of arms of polymer

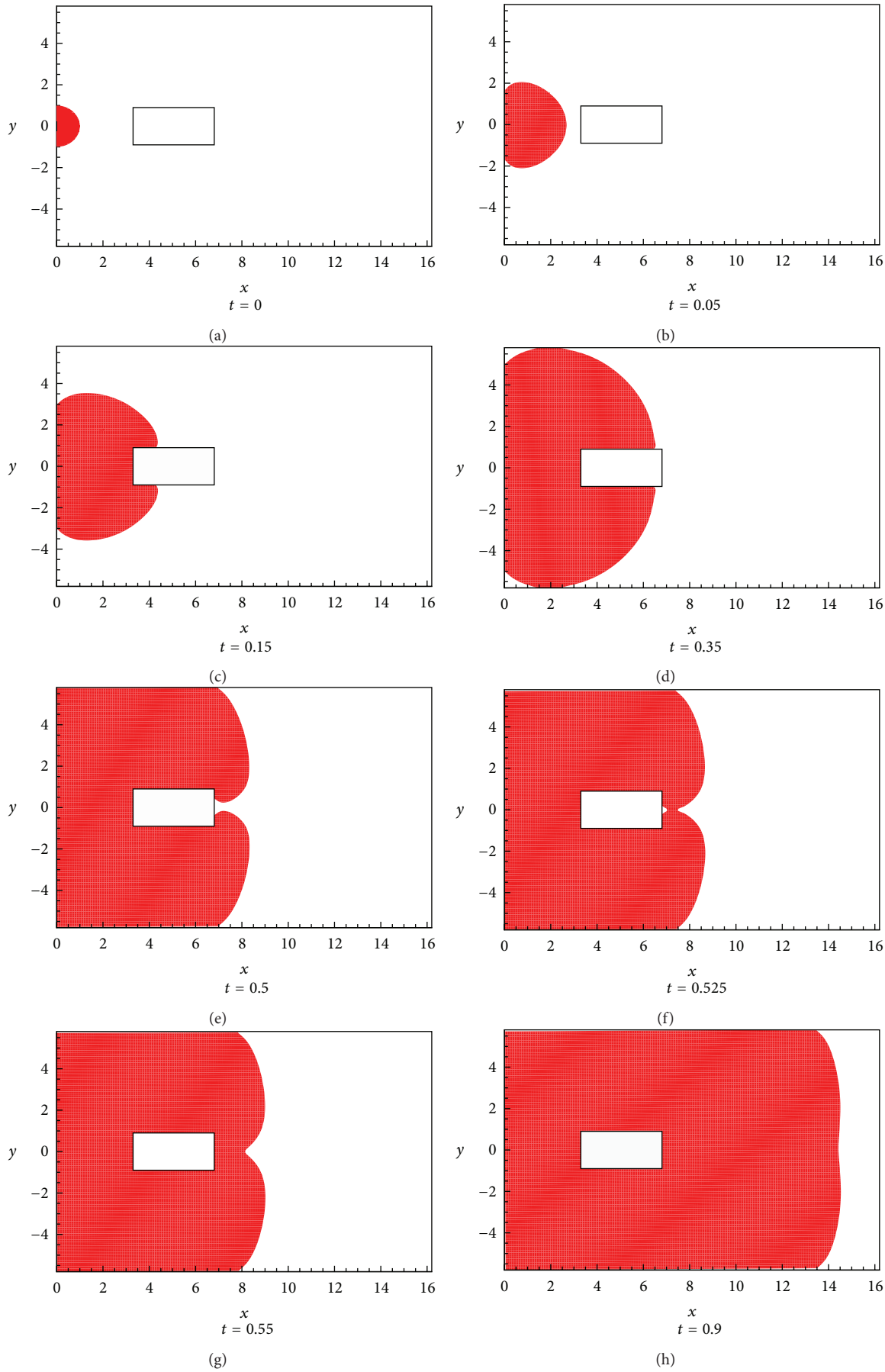

Figure 3: Continued.

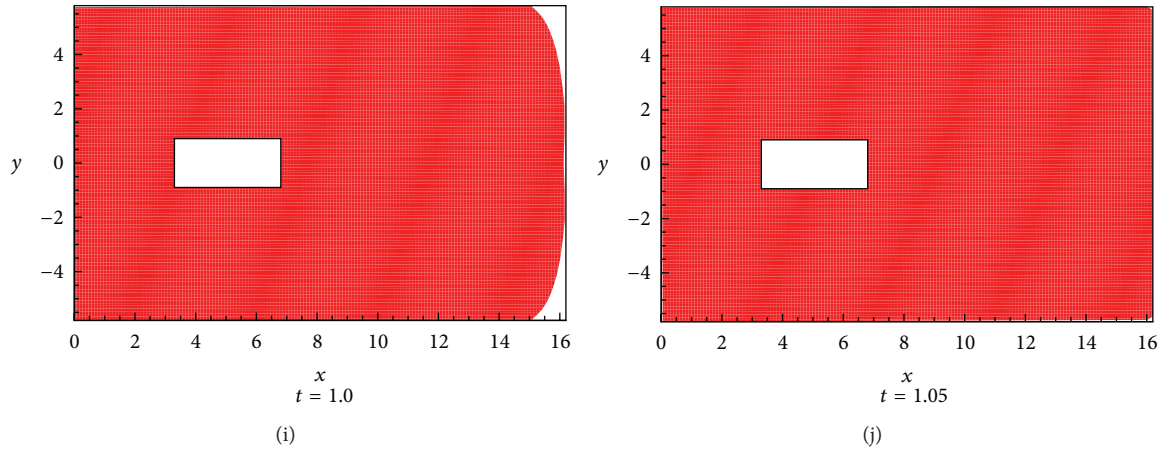

Figure 3: Melt positions at different time in the mold filling process.

chains and **d** is the strain tensor. Some hints on choosing meaningful values of the parameters in XPP model can be found in [25]; in this paper, we take $\beta = 1.0/9.0$, $\alpha = 0.15$, $q = 2.0$, $\varepsilon = 1.0/3.0$.

2.3. Boundary Conditions. Proper boundary conditions must be posed on the solid walls of the cavity. In this paper, no-slip boundary conditions are used for the velocities, that is, $u = v = 0$. As for the pressure boundary conditions, for the air in the cavity, we use no-slip boundary conditions, that is, $p = 0$, while for the melt in the cavity, no-penetration boundary conditions are used, that is, $\partial p/\partial \mathbf{n} = 0$.

3. Numerical Methods

Level set evolution equation (1) and the reinitialization equation (2) are solved by the finite difference method on a rectangular grid. The spatial derivatives are discretized by the 5th-order weighted essentially non-oscillatory (WENO) scheme [29, 30] and the temporal derivatives are discretized by the 3rd-order total variation diminishing Runge-Kutta (TVD-R-K) scheme [31].

The finite volume SIMPLE methods on a nonstaggered grid are used to solve the governing equations (5)–(8).

The validity of the methods has been verified in [23].

4. Numerical Results and Analysis

4.1. Mold Filling Process. Figure 1 shows the sketch map of the mold with an insert in. Figure 2 gives the top view of the mold, which also represents the computational area. In this paper, we take $x = 16.2$, $y = 11.6$, $a = 3.3$, $b = 3.4$, $c = 4.9$, $d = 1.8$, which are the same as those in [26]. The inlet lies in the middle of the left wall of the computational area. The grid number is 200×120.

Figure 3 gives the melt interface positions at different times in mold filling process.

From Figure 3 we can see that the melt is divided into two streams when it reaches the insert. The two streams move forward until they pass the insert; then they begin to move toward each other until they meet at some point behind the insert, from where the weld line begins to form, and a hole appears between the insert and the meet point of the two streams of melt. After meeting, the melt moves toward two opposite directions. One direction is moving forward and the other direction is moving backward to fill in the hole formed between the insert and the meeting point. The hole is finally filled with melt and two streams of melt reunion into one stream and move forward. Figure 4 gives the comparison between the interface evolution after the insert and that obtained in te experiment [26]. The well agreement shows the validity of our model and method.

4.2. Distribution of the Stress Birefringence. In order to get the stress distribution and make a comparison with the experimental results given by the stress birefringence distribution, we use the formula in [32] to compute the numerical stress birefringence, which is given as follows:

$$\Delta n = C\left[\left(\tau_{xx} - \tau_{yy}\right)^2 + 4\tau_{xy}^2\right]^{1/2}. \tag{9}$$

Here, Δn is the stress birefringence. C is the stress-optical coefficient, which is a constant for linear stress-optical principle, and we take $C = 1$.

Figure 5 shows the distribution of the stress birefringence at $t = 1.05$ in the simulation. We can see that the stress birefringence distribution is anisotropic near the weld line district and varies greatly at different positions of the weld line district. This phenomenon is induced by the complicated flow behavior after the two streams of melt meet. Since the melt moves toward two opposite directions, the stress birefringence distribution decreases progressively along the two opposite directions. The stress distribution birefringence obtained in experiment after the product is completely produced is given in Figure 6 [26], Since only the mold filling process is considered in the simulation, while the birefringence is obtained after the cooling stage, some difference exists between the numerical and experimental

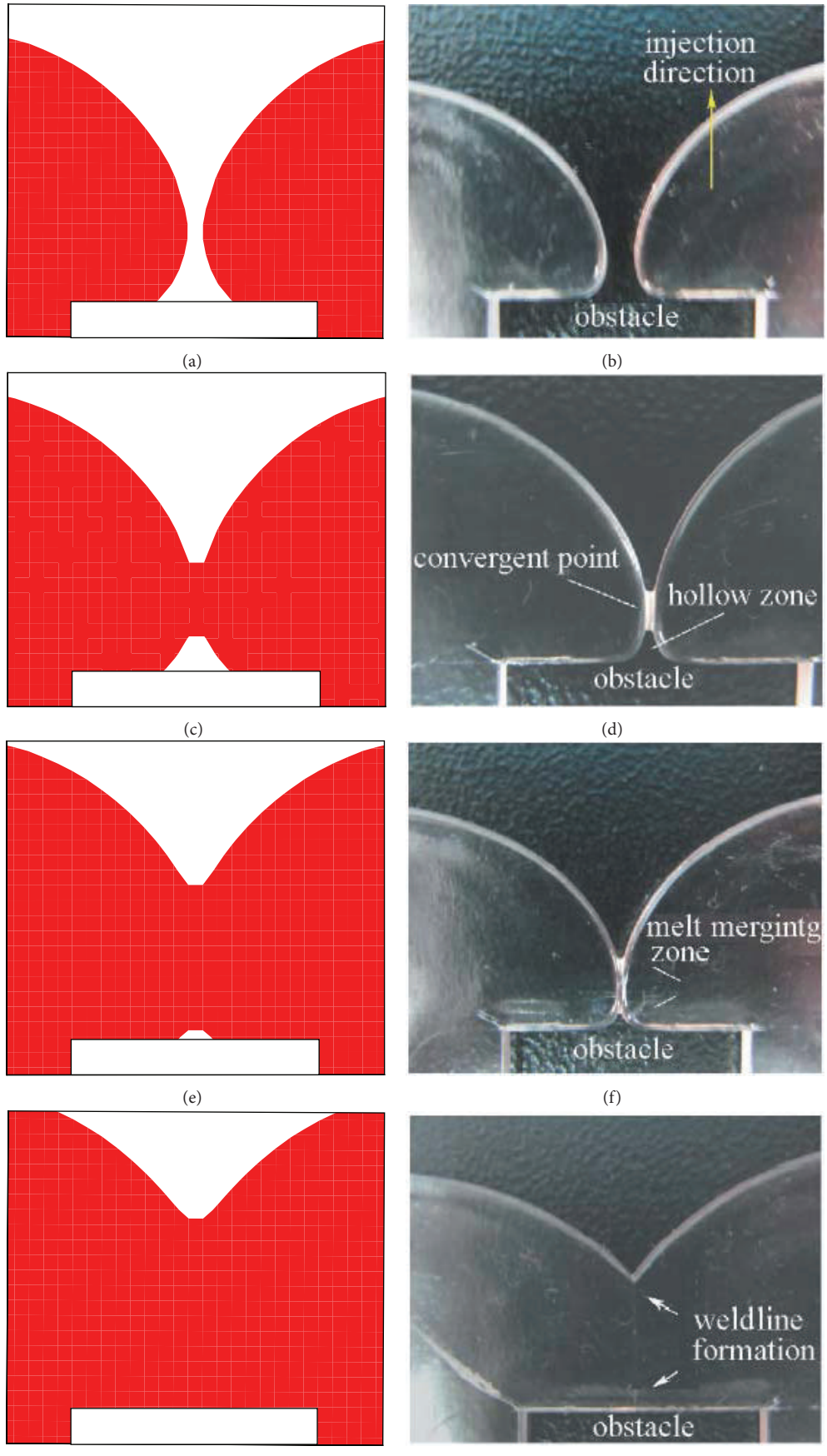

Figure 4: Comparison between the interface evolution after the insert and that obtained in experiment.

Table 1: Definition of the constants and functions in the constitutive equation [24, 25].

Equation	ϖ	ψ	Λ	S_ψ
τ_{xx} normal stress	We	τ_{xx}	0	$2(1-\beta)\frac{\partial u}{\partial x} + 2\mathrm{We}\,\tau_{xx}\frac{\partial u}{\partial x} + 2\mathrm{We}\,\tau_{xy}\frac{\partial u}{\partial y} - f(\lambda,\boldsymbol{\tau})\tau_{xx} - [f(\lambda,\boldsymbol{\tau})-1]\frac{1-\beta}{\mathrm{We}} - \alpha\frac{\mathrm{We}}{1-\beta}\left(\tau_{xx}^2+\tau_{xy}^2\right)$
τ_{xy} shear stress	We	τ_{xy}	0	$(1-\beta)\left(\frac{\partial v}{\partial x}+\frac{\partial u}{\partial y}\right) + \mathrm{We}\,\tau_{xx}\frac{\partial v}{\partial x} + \mathrm{We}\,\tau_{yy}\frac{\partial u}{\partial y} - f(\lambda,\boldsymbol{\tau})\tau_{xy} - \alpha\frac{\mathrm{We}}{1-\beta}\tau_{xy}\left(\tau_{xx}+\tau_{yy}\right)$
τ_{yy} normal stress	We	τ_{yy}	0	$2(1-\beta)\frac{\partial v}{\partial y} + 2\mathrm{We}\,\tau_{yy}\frac{\partial v}{\partial y} + 2\mathrm{We}\,\tau_{xy}\frac{\partial v}{\partial x} - f(\lambda,\boldsymbol{\tau})\tau_{yy} - [f(\lambda,\boldsymbol{\tau})-1]\frac{1-\beta}{\mathrm{We}} - \alpha\frac{\mathrm{We}}{1-\beta}\left(\tau_{yy}^2+\tau_{xy}^2\right)$
τ_{zz} stress	We	τ_{zz}	0	$-f(\lambda,\boldsymbol{\tau})\tau_{zz} - [f(\lambda,\boldsymbol{\tau})-1]\frac{1-\beta}{\mathrm{We}} - \alpha\frac{\mathrm{We}}{1-\beta}\tau_{zz}^2$

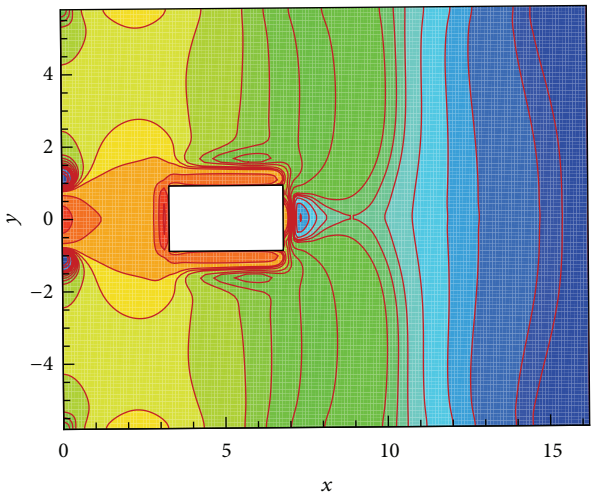

Figure 5: The distribution of the stress birefringence at $t = 1.05$ in the simulation.

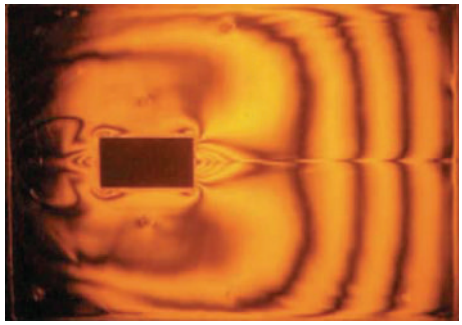

Figure 6: The stress distribution birefringence obtained in experiment [26] after the product is completely produced.

results. However, both the numerical and the experimental results are qualitative agreeable.

Figure 7 gives the change of the stress birefringence from the tail of the insert until the end of the cavity, which is in accordance qualitatively with the experiment in [26], that

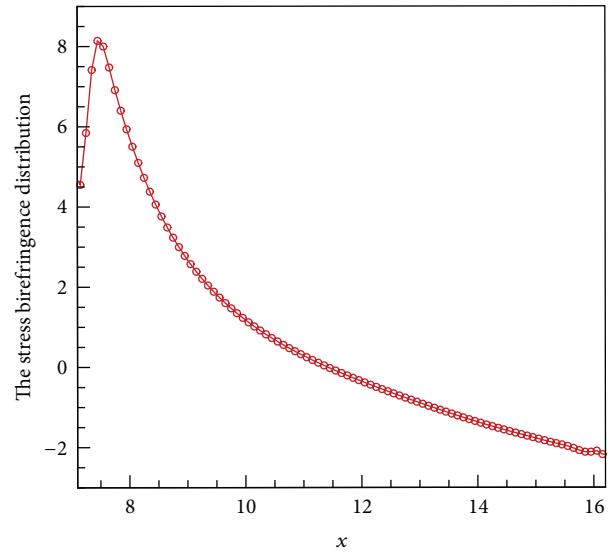

Figure 7: The change of the stress birefringence from the tail of the insert until the end of the cavity.

is, the stress birefringence increases quickly near the weld line district and then decreases gradually until reaching the tail of the mold cavity. The maximum value of the stress birefringence appears at some point after the insert.

5. Conclusion

In this paper, simulations of interface evolution and stress distribution near weld line in the viscoelastic melt mold filling process are achieved according to the viscoelastic-Newtonian two-phase model established by Yang et al. [23]. The interface evolution of the viscoelastic melt in the mold filling process with an insert in is captured accurately. The distribution of the stress birefringence is qualitative agreeable with that of experiment. The stress increases quickly near the weld line district and then decreases gradually until reaching the

tail of the mold cavity. The maximum value of the stress birefringence appears at some point after the insert.

Acknowledgments

All the authors would like to acknowledge the National Natural Science Foundation of China (10871159), National Natural Science Foundation of Shanxi (2012011019-2), and Doctoral Foundation of Taiyuan University of Science and Technology (20112011).

References

[1] V. W. Wang, C. A. Hieber, and K. K. Wang, "Dynamic simulation and graphics for the injection-molding of 3-dimensional thin parts," *Journal of Polymer Engineering*, vol. 7, no. 1, pp. 21–45, 1986.

[2] H. H. Chiang, C. A. Hieber, and K. K. Wang, "A unified simulation of the filling and post filling stages in injection molding. Part I. Formulation," *Polymer Engineering and Science*, vol. 31, no. 2, pp. 116–123, 1991.

[3] K. K. Kabanemi, H. Vaillancourt, H. Wang, and G. Salloum, "Residual stresses, shrinkage, and warpage of complex injection molded products: numerical simulation and experimental validation," *Polymer Engineering and Science*, vol. 38, no. 1, pp. 21–37, 1998.

[4] D. E. Smith, D. A. Tortorelli, and C. L. Tucker III, "Analysis and sensitivity analysis for polymer injection and compression molding," *Computer Methods in Applied Mechanics and Engineering*, vol. 167, no. 3-4, pp. 325–344, 1998.

[5] J. F. Hétu, D. M. Gao, A. Garcia-Rejon, and G. Salloum, "3D finite element method for the simulation of the filling stage in injection molding," *Polymer Engineering and Science*, vol. 38, no. 2, pp. 223–236, 1998.

[6] E. Pichelin and T. Coupez, "Finite element solution of the 3D mold filling problem for viscous incompressible fluid," *Computer Methods in Applied Mechanics and Engineering*, vol. 163, no. 1–4, pp. 359–371, 1998.

[7] S. W. Kim and L. S. Turng, "Three-dimensional numerical simulation of injection molding filling of optical lens and multiscale geometry using finite element method," *Polymer Engineering and Science*, vol. 46, no. 9, pp. 1263–1274, 2006.

[8] H. M. Zhou, T. Geng, and D. Q. Li, "Numerical filling simulation of injection molding based on 3D finite element model," *Journal of Reinforced Plastics and Composites*, vol. 24, no. 8, pp. 823–830, 2005.

[9] R. Y. Chang and W. H. Yang, "Numerical simulation of mold filling in injection molding using a three-dimensional finite volume approach," *International Journal for Numerical Methods in Fluids*, vol. 37, no. 2, pp. 125–148, 2001.

[10] J. Zhou and L. S. Turng, "Three-dimensional numerical simulation of injection mold filling with a finite-volume method and parallel computing," *Advances in Polymer Technology*, vol. 25, no. 4, pp. 247–258, 2006.

[11] B. X. Yang, J. Ouyang, C. T. Liu, and Q. Li, "Simulation of non-isothermal injection molding for a non-newtonian fluid by Level Set method," *Chinese Journal of Chemical Engineering*, vol. 18, no. 4, pp. 600–608, 2010.

[12] E. J. Holm and H. P. Langtangen, "A unified finite element model for the injection molding process," *Computer Methods in Applied Mechanics and Engineering*, vol. 178, no. 3-4, pp. 413–429, 1999.

[13] J. A. Luoma and V. R. Voller, "An explicit scheme for tracking the filling front during polymer mold filling," *Applied Mathematical Modelling*, vol. 24, no. 8-9, pp. 575–590, 2000.

[14] S. Soukane and F. Trochu, "Application of the level set method to the simulation of resin transfer molding," *Composites Science and Technology*, vol. 66, no. 7-8, pp. 1067–1080, 2006.

[15] R. Ayad and A. Rigolot, "The VOF-G/FEV model for tracking a polymer-air interface in the injection moulding process," *Journal of Mechanical Design*, vol. 124, no. 4, pp. 813–821, 2002.

[16] G. Tie, L. Dequn, and Z. Huamin, "Three-dimensional finite element method for the filling simulation of injection molding," *Engineering with Computers*, vol. 21, no. 4, pp. 289–295, 2006.

[17] M. S. Kim, J. S. Park, and W. I. Lee, "A new VOF-based numerical scheme for the simulation of fluid flow with free surface. Part II: application to the cavity filling and sloshing problems," *International Journal for Numerical Methods in Fluids*, vol. 42, no. 7, pp. 791–812, 2003.

[18] H. M. Zhou, B. Yan, and Y. Zhang, "3D filling simulation of injection molding based on the PG method," *Journal of Materials Processing Technology*, vol. 204, no. 1–3, pp. 475–480, 2008.

[19] C. K. Au, "A geometric approach for injection mould filling simulation," *International Journal of Machine Tools and Manufacture*, vol. 45, no. 1, pp. 115–124, 2005.

[20] B. X. Yang, J. Ouyang, S. P. Zheng, Q. Li, and W. Zhou, "Simulation of polymer molding filling process with an adaptive weld line capturing algorithm," *International Journal of Material Forming*, vol. 5, no. 1, pp. 25–37, 2012.

[21] A. Bonito, M. Picasso, and M. Laso, "Numerical simulation of 3D viscoelastic flows with free surfaces," *Journal of Computational Physics*, vol. 215, no. 2, pp. 691–716, 2006.

[22] M. F. Tomé, A. Castelo, J. Murakami et al., "Numerical simulation of axisymmetric free surface flows," *Journal of Computational Physics*, vol. 157, no. 2, pp. 441–472, 2000.

[23] B. X. Yang, J. Ouyang, Q. Li, Z. F. Zhao, and C. T. Liu, "Modeling and simulation of the viscoelastic fluid mold filling process by level set method," *Journal of Non-Newtonian Fluid Mechanics*, vol. 165, no. 19-20, pp. 1275–1293, 2010.

[24] M. Aboubacar, J. P. Aguayo, P. M. Phillips et al., "Modelling Pom-Pom type models with high-order finite volume schemes," *Journal of Non-Newtonian Fluid Mechanics*, vol. 126, no. 2-3, pp. 207–220, 2005.

[25] M. G. H. M. Baltussen, W. M. H. Verbeeten, A. C. B. Bogaerds, M. A. Hulsen, and G. W. M. Peters, "Anisotropy parameter restrictions for the eXtended Pom-Pom model," *Journal of Non-Newtonian Fluid Mechanics*, vol. 165, no. 19-20, pp. 1047–1054, 2010.

[26] J. Han, C. Y. Shen, C. T. Liu, S. J. Wang, and J. B. Chen, "Flow induced birefringence of weldline region in polystyrene injection molding," *CIESC Journal*, vol. 59, no. 5, pp. 1305–1309, 2008.

[27] M. Sussman, E. Fatemi, P. Smereka, and S. Osher, "An improved level set method for incompressible two-phase flows," *Computers and Fluids*, vol. 27, no. 5-6, pp. 663–680, 1998.

[28] W. M. H. Verbeeten, G. W. M. Peters, and F. P. T. Baaijens, "Differential constitutive equations for polymer melts: the extended Pom-Pom model," *Journal of Rheology*, vol. 45, no. 4, pp. 823–843, 2001.

[29] G. S. Jiang and D. P. Peng, "Weighted ENO schemes for Hamilton—Jacobi equations," *SIAM Journal on Scientific Computing*, vol. 21, no. 6, pp. 2126–2143, 2002.

[30] S. Osher and C. W. Shu, "High-order essentially non-oscillatory schemes for Hamilton-Jacobi equations," *SIAM Journal on Numerical Analysis*, vol. 28, no. 4, pp. 907–922, 1991.

[31] C. W. Shu and S. Osher, "Efficient implementation of essentially non-oscillatory shock-capturing schemes II," *Journal of Computational Physics*, vol. 83, no. 1, pp. 32–78, 1989.

[32] A. I. Isayev, G. D. Shyu, and C. T. Li, "Residual stresses and birefringence in injection molding of amorphous polymers: simulation and comparison with experiment," *Journal of Polymer Science B*, vol. 44, no. 3, pp. 622–639, 2006.